Magnetic-field-induced domain-wall motion in permalloy nanowires with modified Gilbert damping

Thomas A. Moore,* Philipp Möhrke, Lutz Heyne, Andreas Kaldun, and Mathias Kläui†
Fachbereich Physik, Universität Konstanz, Universitätsstrasse 10, 78457 Konstanz, Germany

Dirk Backes,‡ Jan Rhensius,‡ and Laura J. Heyderman
Laboratory for Micro- and Nanotechnology, Paul Scherrer Institut, 5232 Villigen PSI, Switzerland

Jan-Ulrich Thiele
San Jose Research Center, Hitachi Global Storage Technologies, San Jose, California 95135, USA

Georg Woltersdorf
Fakultät für Physik, Universität Regensburg, Universitätsstrasse 31, 93040 Regensburg, Germany

Arantxa Fraile Rodríguez§ and Frithjof Nolting
Swiss Light Source, Paul Scherrer Institut, 5232 Villigen PSI, Switzerland

Tevfik O. Menteş, Miguel Á. Niño, and Andrea Locatelli
Elettra – Sincrotrone Trieste S.C.p.A., 34149 Basovizza, Trieste, Italy

Alessandro Potenza, Helder Marchetto, Stuart Cavill, and Sarnjeet S. Dhesi
Diamond Light Source Ltd., Harwell Science and Innovation Campus, Didcot, Oxfordshire OX11 0DE, United Kingdom
(Received 5 January 2010; revised manuscript received 13 July 2010; published 28 September 2010)

Domain wall (DW) depinning and motion in the viscous regime induced by magnetic fields, are investigated in planar permalloy nanowires in which the Gilbert damping α is tuned in the range 0.008–0.26 by doping with Ho. Real time, spatially resolved magneto-optic Kerr effect measurements yield depinning field distributions and DW mobilities. Depinning occurs at discrete values of the field which are correlated with different metastable DW states and changed by the doping. For $\alpha < 0.033$, the DW mobilities are smaller than expected while for $\alpha \geq 0.033$, there is agreement between the measured DW mobilities and those predicted by the standard one-dimensional model of field-induced DW motion. Micromagnetic simulations indicate that this is because as α increases, the DW spin structure becomes increasingly rigid. Only when the damping is large can the DW be approximated as a pointlike quasiparticle that exhibits the simple translational motion predicted in the viscous regime. When the damping is small, the DW spin structure undergoes periodic distortions that lead to a velocity reduction. We therefore show that Ho doping of permalloy nanowires enables engineering of the DW depinning and mobility, as well as the extent of the viscous regime.

DOI: 10.1103/PhysRevB.82.094445 PACS number(s): 75.78.Fg, 75.78.Cd, 75.50.Bb

I. INTRODUCTION

Domain wall (DW) propagation in magnetic nanowires[1,2] holds both fundamental interest and the potential for applications in logic and memory devices.[3,4] In the commonly studied planar permalloy wires ($Ni_{80}Fe_{20}$,Py), where the width of the wire is much larger than the thickness, two types of DW spin structure are stable at zero field:[5,6] transverse walls (TW) in thinner and narrower wires and vortex walls (VW) in thicker and wider wires. Applying a magnetic field H along the axis of the wire causes the DW to propagate in the field direction to minimize the Zeeman energy,[7,8] and for sufficiently low H this process is well described by a one-dimensional (1D) model originally developed for Bloch-type DWs (Refs. 9 and 10) that predicts a linear dependence of the DW velocity on the field ($v = \mu H$, where $\mu = \gamma\Delta/\alpha$ is the DW mobility, γ is the gyromagnetic ratio, Δ the DW width and α the Gilbert damping constant). In this low field, viscous regime the DW spin structure is preserved.[11] At a critical (Walker threshold) field H_W, which is directly proportional to α and the saturation magnetization M_S, the average DW velocity is drastically reduced,[9–12] accompanied by an oscillatory motion of the DW and transformations of the DW spin structure (in Py, from TW to VW or antivortex wall, and vice versa). Temporal oscillations of the nanowire resistance showed that these DW transformations contain a periodic component[13,14] and the accompanying velocity oscillations have been detected by time-resolved magneto-optic Kerr effect (MOKE) measurements.[15] Subsequently, a loss of periodicity in the DW transformations due to interlayer magnetic interactions and edge roughness was demonstrated in a single shot experiment on a Py wire in a multilayer stack.[16] A further increase in the field leads eventually to a second linear motion regime,[9–12] where the DW motion is predicted to occur via the serial processes of nucleation, gyrotropic motion and annihilation of vortex-antivortex pairs.[17]

There is growing interest in trying to prevent the DW transformations and consequent velocity breakdown at H_W in order to extend the range of H for which simple translational

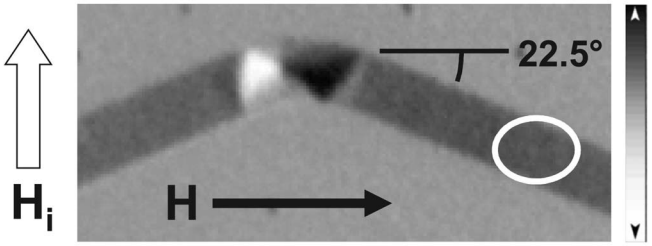

FIG. 1. XMCD-PEEM image of a DW (vortex-type) positioned at a bend in a 1500 nm-wide, zig-zag Py wire by an initializing field H_i. Magnetic contrast is in the vertical direction (see contrast strip on the right). A propagation field H is applied at 22.5° to the zig-zag branches. The DW subsequently passes through a MOKE laser spot (white ring).

DW motion occurs, making magnetic nanowires more attractive for use in devices. Several methods have been proposed or demonstrated, including introducing an underlayer with large perpendicular magnetic anisotropy,[18] adding a perpendicular[19] or transverse bias field,[20] engineering the wire geometry[21] or even exploiting the natural edge roughness.[22] At the same time there is a drive to control the DW depinning from thermally stable positions or pinning sites, e.g., by tuning the wire geometry.[23] In this work we investigate the effect on DW depinning and motion of systematically modifying the damping, achieved by doping Py nanowires with Ho.[24] Although increasing α is predicted to have little effect on the depinning field[25] and to reduce the DW velocity, it is also expected to postpone the onset of DW transformations to higher fields.[9,10] We report on depinning at discrete values of field which correlate with different metastable DW states and are changed by the Ho doping. The measured DW mobility agrees with the 1D model only for large α and comparison with micromagnetic simulations indicates that α-dependent DW spin structure distortions account for this discrepancy.

II. EXPERIMENTAL METHOD

We study Py zig-zag wires of 1500 nm width, 20 nm thickness and length approximately 80 μm fabricated on Si substrates by electron-beam lithography and lift-off. The damping α was controlled by codepositing the Py with Ho,[24] and nanowires of five different compositions were obtained: pure Py and Py doped with 1, 2, 4 and 10 at. % Ho, hereafter referred to as Py(0Ho), Py(1Ho), etc. Ferromagnetic resonance measurements were used to determine α as 0.008, 0.02, 0.033, 0.087, and 0.26, respectively. Adding Ho reduces M_S by 5% per at. % Ho due to antiferromagnetic coupling between the rare earth sublattice and the Py.[26]

To investigate DW motion in the nanowires, we use a real time focused MOKE technique as described in Ref. 27. A DW is positioned at a bend in the nanowire (Fig. 1) by applying and subsequently reducing to zero an initializing field H_i in plane and perpendicular to the wire. In this wire geometry, VWs have the lowest energy and while TWs may arise directly after initialization, they relax immediately to the vortex-type as soon as fields are applied.[6] A field H used to propagate the DW is ramped linearly from zero to 50 G in 50 μs. The DW velocity is deduced from the time T taken by the DW to transit a focused laser spot of known diameter positioned 10 μm from the bend. The depinning field is deduced from the time of arrival of the DW at the laser spot (t_0), which is possible because the evolution of the field with time is known, and the field sweep on the scale of tens of μs is slow compared to the ~100 ns required for the DW to reach the laser spot.[27] We repeat the DW initialization and propagation through the laser spot approximately 200 times for each nanowire and determine the depinning field distribution and mobility.

III. DOMAIN WALL DEPINNING

The distributions of DW depinning fields for Py wires of each composition obtained in the experiment are plotted in Fig. 2. The dominant feature of this data is that, even though the DWs are prepared in nominally identical ways, depinning occurs at different fields and even clusters at certain values of field, meaning that there are a few discrete field values at which a wall can depin. These depinning clusters or "channels" are particularly apparent for Py(1Ho) and Py(2Ho). Since the depinning field is directly proportional to the time of arrival of the DW at the laser spot, this data suggests that some DWs may take more time to reach the laser spot than others due to different paths taken through the energy landscape, e.g., as the fine structure of the DW is constantly evolving due to thermal fluctuations, on some passes the DW could interact more strongly with a wire defect that pins it for a longer time than on other passes. However, perhaps a more likely explanation stems from the different metastable states of the DW that could arise when it is prepared at the bend in the wire. Hayashi *et al.*[28] found four distinct states of a DW trapped at an artificial pinning site in a Py wire, corresponding to two TWs and two VWs, each with either clockwise or counterclockwise circulation, requiring different depinning fields. In our case both clockwise and counterclockwise VWs are possible but only one orientation of the TW is allowed; that with the magnetization at the DW center pointing in the direction of the initializing field. Evidence for this is that these three DW structures have been observed in similar zig-zag wires by x-ray magnetic circular dichroism photoemission electron microscopy (XMCD-PEEM) (Ref. 29) and three distinct depinning channels have been observed before in pure Py wires using the same focused MOKE setup.[27] The details of the depinning field distribution appear to depend strongly not only on the sample composition, as indicated by the variety of distributions in Fig. 2 but also on its geometry. For example, the pure Py wire [Py(0Ho)] differs only by 5 nm in thickness from a similar wire investigated in Ref. 27, and yet there is a significant reduction in the discreteness of the depinning channels.

For Py(1Ho), there are three distinct depinning channels, with two or three for Py(2Ho) and two (albeit closely spaced) for Py(4Ho). For Py(10Ho), only one depinning channel is evident, although it should be noted that here only a limited number of measurements were possible due to the difficulty of obtaining a large enough Kerr signal. In Fig. 2 each chan-

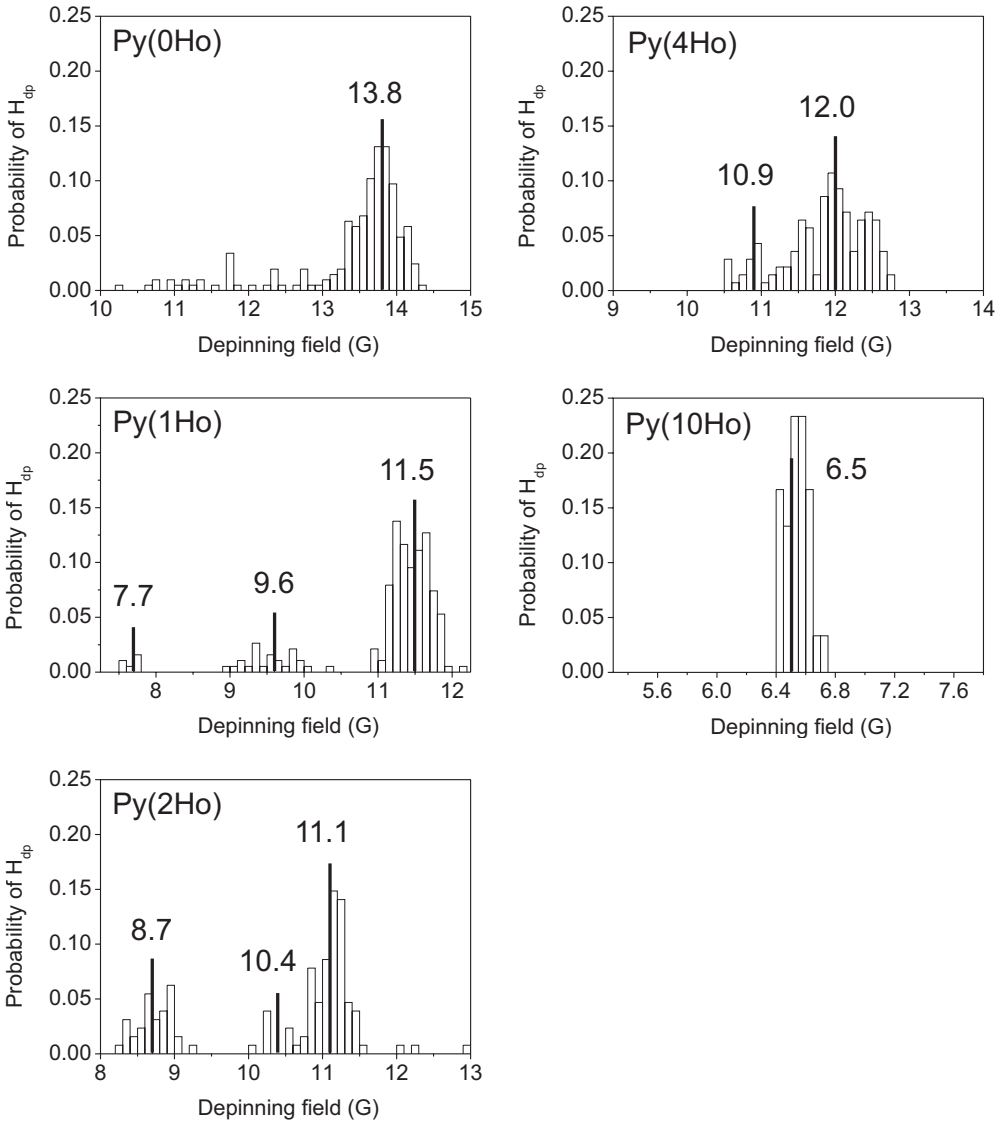

FIG. 2. Probability distributions of the depinning field H_{dp} of a DW in 1500 nm-wide, 20 nm-thick Py wires doped with Ho. Pure Py =Py(0Ho), Py doped with 1 at. % Ho=Py(1Ho), etc.

nel is marked with its average depinning field. The number of depinning channels is in good agreement with observations by XMCD-PEEM, represented in a probability chart in Fig. 3, which show that while VWs of both chirality and TWs appear after initialization in Py(1Ho) and Py(2Ho), the TWs are extremely rare for Py(4Ho) (thus the third channel is lost), and in Py(10Ho), while VWs of both circulation remain, TWs are never seen. The question remains why the two depinning channels corresponding to the VWs of different circulation should converge to a unique depinning field as the Ho doping increases from 4 to 10 at. %. This detail suggests that the depinning barriers for the two VWs become closer in energy as the Ho content increases.

In order to better understand the DW depinning, we performed micromagnetic simulations[30] (Fig. 4). A section of the Py wire at a bend was reproduced, a clockwise and a counterclockwise VW were prepared in turn, and a magnetic field applied in the same direction as in the experiment (compare Fig. 1) was gradually increased until the DWs exited the bend. The simulation parameters for Py(0Ho) were $\alpha = 0.008$, $M_S = 800$ kA/m, exchange constant $A = 13 \times 10^{-12}$ J/m, magnetocrystalline anisotropy $K = 0$ and cell size 5 nm. For Py(0Ho), the clockwise and counterclockwise VWs depinned abruptly at 13.1 G and 25.6 G, respectively. Figure 4 illustrates the DW spin configurations. The simulations were repeated for wires of all compositions, varying α and M_S as appropriate. The exchange constant was not adjusted, as simulations showed that reducing A on the order of the doping concentration (i.e., up to 10%, a "worst case" scenario) did not produce any change in the depinning field. The depinning fields are plotted in Fig. 5(a) as a function of Ho content. The third DW configuration, a TW, always transformed to a VW before depinning, making a third depinning channel impossible to reproduce. While in the experiment, TWs, observed as one of the three metastable DW states, require a certain field in order to depin, and subsequently transform, in the simulation an immediate transformation from TW to VW is permitted.

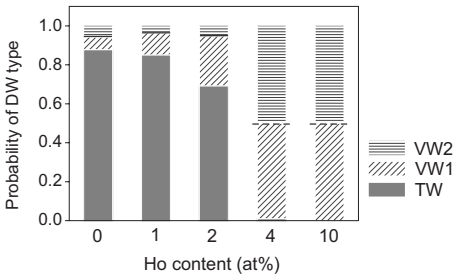

FIG. 3. Probability of finding transverse walls (TWs) and vortex walls (VWs) after initialization, for each wire composition, measured by XMCD-PEEM imaging. The two VW chiralities are labeled VW1, VW2 (clockwise and counterclockwise). In Py(4Ho) and Py(10Ho) both VW chiralities were seen but their probabilities are not accurately known due to the small number of initializations performed for these samples.

Comparing our results with those of Hayashi *et al.*,[28] the TW is expected to have the largest depinning field. This, together with the fact that TWs are the commonest DW type in Py(0Ho), Py(1Ho), and Py(2Ho) (Fig. 3), is consistent with the largest cluster of depinning fields being at the highest field in each case (13.8 G, 11.5 G, and 11.1 G, respectively). The growing dominance of clusters at lower fields as the Ho content increases can be ascribed to the increasing number of VWs observed at initialization. For Py(4Ho) and Py(10Ho), TWs are very unlikely and so the depinning field clusters must be generated almost entirely by the depinning of VWs. Experimental depinning fields for the various DW configurations in each wire are depicted in Fig. 5(b). Here we have assumed that VWs with counterclockwise circulation depin at higher fields than VWs with clockwise circulation, in line with our simulation.

Comparing simulation and experiment, we see that in both cases across the full Ho doping range 0–10 at. % the depinning field averaged over all DW types tends to decrease with increasing Ho content [open squares in Figs. 5(a) and 5(b)]. In this way the depinning field behaves similarly to the threshold current density j_c for DW motion in the same wires.[31] The decrease in M_S with increasing Ho content is the

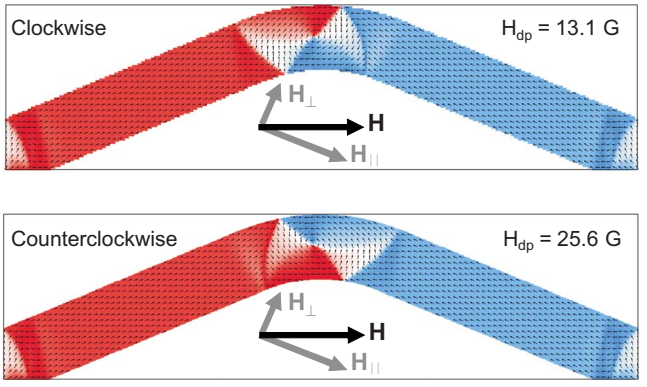

FIG. 4. (Color online) Simulated spin configurations of (i) a clockwise and (ii) a counterclockwise VW positioned at a bend in a 1500 nm-wide, zig-zag, pure Py wire. The DWs depin abruptly at the fields indicated. Components of the applied field transverse ($H_\perp$) and parallel ($H_\parallel$) to the right branch of the wire are indicated.

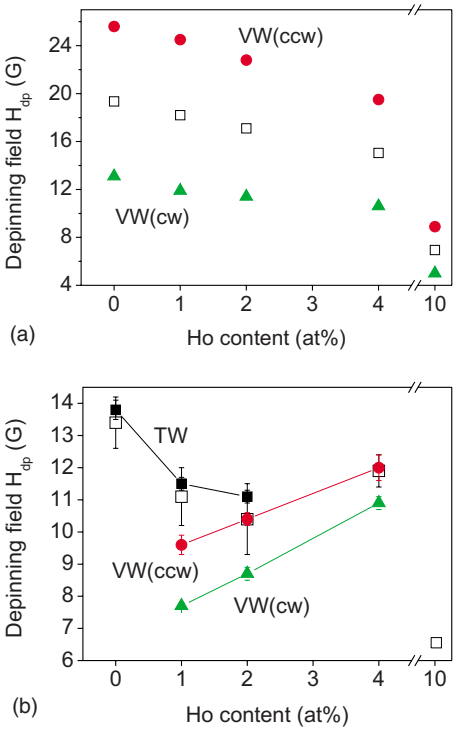

FIG. 5. (Color online) (a) Depinning fields H_{dp} for clockwise and counterclockwise vortex walls as a function of Ho content, from simulation. Open squares represent the depinning field averaged over the two VW types. (b) Depinning fields H_{dp} for the various DW spin structures as a function of Ho content, from experiment. TW=transverse wall (solid squares), VW(ccw)=counterclockwise vortex wall (circles), VW(cw)=clockwise vortex wall (triangles). Open squares represent the depinning field averaged over all DW types. The error bars are the standard deviations of the associated depinning field clusters. For Py doped with 10 at. % Ho there is only one depinning field cluster, represented by its average value.

probable cause of the drop in depinning field. For Ho doping between 1 and 4 at. %, the depinning fields of the VWs decrease in the simulation but increase in the experiment. We expect that this difference is due to extrinsic pinning, which is not accounted for in the simulation. Meanwhile, the difference in depinning field between the two VW types decreases as the Ho content increases in both the simulation and the experiment. The demagnetizing energy and the Zeeman energy both depend on M_S, which decreases, and the simulations show that the Zeeman energy undergoes a larger decrease for the counterclockwise VW than for the clockwise VW as the Ho content is increased, leading to the convergence of the VW depinning fields

For Ho doping from 0 to 2 at. %, the depinning field of the TW decreases as the Ho doping increases. The TW has a large magnetostatic field, which can help to pin it at edge defects or, as in this case, at the bend in the wire. A reduction in M_S decreases this magnetostatic field and thereby the depinning field.

IV. DOMAIN WALL MOTION

The experiment shows that the time T for the DW to transit the laser spot, and thus the DW velocity, has a distri-

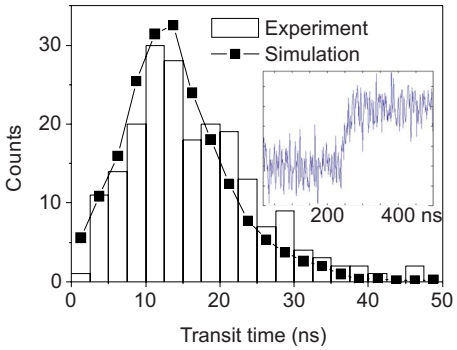

FIG. 6. (Color online) Distribution of laser spot transit times for DW motion in a pure Py wire. The columns are the experimental data, normalized to a depinning field of 11 G. The squares are simulation data, obtained by analyzing 5000 simulated Kerr signals with signal-to-noise ratio as in the experiment. The inset shows a simulated Kerr signal.

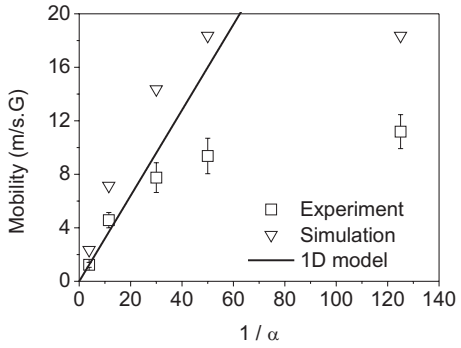

FIG. 7. DW mobility as a function of $1/\alpha$ for 1500 nm-wide, 20 nm-thick Py wires doped with Ho determined by real time MOKE (squares) and micromagnetic simulation (down triangles). The solid line is the prediction from the 1D model $v=(\gamma\Delta/\alpha)H$, with $\gamma=176$ GHz/T and $\Delta=20$ nm (the "effective width" of a VW).

bution. The distribution of T for the pure Py wire is shown in Fig. 6: the most common transit time is 11 ± 1 ns. To understand the shape of this distribution we performed an analysis of simulated MOKE data. 5000 model Kerr signals with identical transit times of 11 ns were superimposed with Gaussian white noise of the same amplitude as in the experiment (signal-to-noise ratio 1:1). The inset of Fig. 6 shows an example of a simulated Kerr signal. Fitting with an error function to obtain T in the same way as in the experiment,[27] we obtain a distribution of T that matches very well the shape of the experimental distribution (Fig. 6). The peak transit time of the simulated distribution is $T_{pk}=11\pm1$ ns, obtained by curve fitting (where the precise fit function is unimportant due to the 2 ns histogram bin size and correspondingly large uncertainty). We conclude that while the broadening is due to the noise level of the measurement, T_{pk} of the experimental distribution is a suitable value to use in calculating the DW velocity because in the simulation the underlying transit time of 11 ns correlates to the peak of the distribution and survives the addition of the noise.

The DW mobility is determined from the ratio of velocity to field. To find the average DW mobility in a given wire we use the average of the depinning field distribution. The mobility is shown in Fig. 7 as a function of $1/\alpha$ (squares), and it tends to decrease with increasing α, in qualitative agreement with the 1D model. Plotting the 1D model prediction (solid line) we also find a fairly good quantitative agreement but only for $\alpha\geq0.033$.

In order to understand the discrepancy between theory and experiment in Fig. 7, we turn to micromagnetic simulations of DW motion.[32] A head-to-head VW was placed in a 10 μm-long Py wire with width, thickness and material parameters the same as in the experiment ($\alpha=0.008-0.26$, $M_S=800-400$ kA/m, $A=13\times10^{-12}$ J/m, $K=0$, cell size 5 nm) and subjected to an applied field of 11 G at an angle of 22.5° to the wire direction, mimicking the experimental geometry. Figure 8(a) shows the DW displacement, proportional to the magnetization along the wire direction M_x, as a function of simulation time. It is seen that, in general, the gradient of $M_x(t)$ and thus the DW velocity decreases with increasing Ho content, in qualitative agreement with the experiment. The simulations also reveal subtle changes in the nature of the DW motion as the Ho content increases, illustrated in Fig. 8(b). For $\alpha=0.008$, 0.02, and 0.033 the vortex core moves toward the upper edge of the wire and toward the leading edge of the DW. For $\alpha=0.008$, the vortex core position oscillates perpendicularly to the wire axis with low amplitude (~100 nm) while the DW moves forward, giving small periodic changes in the gradient of $M_x(t)$ as seen in Fig. 8(a). As α increases, the vortex core tends to remain closer to the center of the DW ($\alpha=0.087$ and 0.26) while the DW moves forward increasingly slowly. For $\alpha=0.26$, the vortex core appears to start moving toward the opposite (lower) edge of the wire and toward the trailing edge of the DW. The simulations also show that transformations of the DW spin structure such as vortex nucleation and annihilation do not occur for any wire composition, suggesting that DW motion remains in the low-field, viscous regime.

In order to compare the simulations with the real time MOKE experiment, we examined the steady state DW motion in each wire (which occurs for $t\geq12$ ns) and calculated the time required for the DW to travel 10 μm (the distance from the DW start position to the laser spot in the experiment). The resulting average DW mobility is shown in Fig. 7 (down triangles).

The DW mobilities as a function of $1/\alpha$ obtained from experiment and simulation are qualitatively similar, showing a reduction in the mobility as α increases. The detailed differences between experiment and simulation are as follows. First, the simulated DW mobilities are larger than the experimental values and by a factor of approximately two for small α. Possible reasons for this are: (i) material inhomogeneities that would reduce the DW mobility are not included in the simulations (as they are inherently unknown) and (ii) the simulations do not account for thermal fluctuations, which are beyond the scope of this study. An investigation of disorder effects on VW propagation by micromagnetic modeling demonstrates that disorder increases effective damping and reduces DW velocity in the viscous regime, and could explain our results.[33] Second, the simulated DW mobilities follow the behavior predicted by the 1D model more closely than the experiment (reasonable agreement occurs up to $1/\alpha=50$ for the simulations but only up to $1/\alpha\approx30$ for the

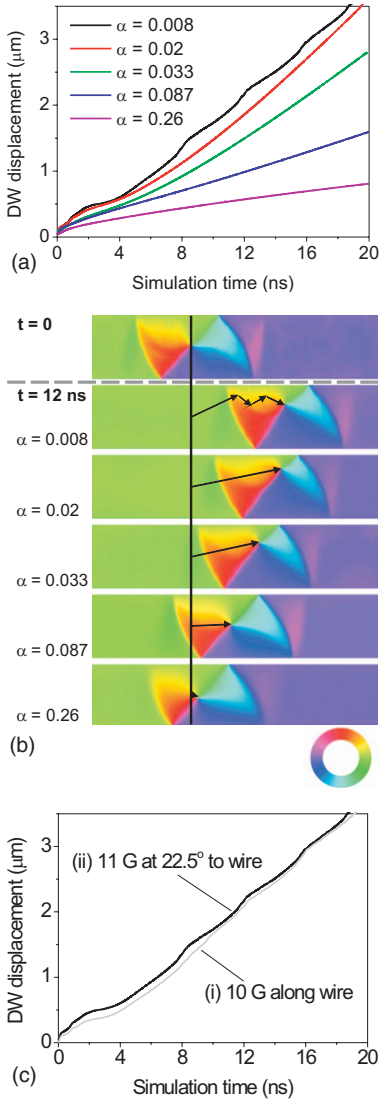

FIG. 8. (Color) (a) DW displacement as a function of time for a micromagnetic simulation of a vortex-type DW propagated by an external field in a 1500 nm-wide, 20 nm-thick Py strip, for different Ho concentrations. (b) Snapshots of the propagating DW from the simulations. At the start the vortex core is in the center of the wall and the wire, and there is no difference in the wall width for different Ho concentrations. The relative displacement and wall spin structure is subsequently shown for each wire at a simulation time $t=12$ ns, when the DW reaches steady state motion. The color wheel indicates the direction of the magnetization. Arrows on the images approximate the vortex core trajectory between $t=0$ and $t=12$ ns. (c) Comparison of the DW displacement in a pure Py strip for two applied fields: (i) 10 G along the wire, and (ii) 11 G at 22.5° to the wire.

experiment). This suggests that, for $\alpha \geq 0.02$ (simulation) and $\alpha \geq 0.033$ (experiment), the DW may be described well as a pointlike quasiparticle. Figure 8(b) shows that this is a good approximation because apart from the initial sideways movement of the vortex core for $\alpha=0.02$ and 0.033, there is very little distortion in the DW spin structure. Finally, for $\alpha=0.008$, the DW mobilities determined from simulation and experiment are both smaller than predicted by the 1D model. This is because the oscillating vortex core emits spin waves that may reduce the efficiency of the field-induced motion.

In simulations of the same pure Py wire but with the field oriented along the wire direction[29] we showed that the Walker breakdown process for this wire geometry involves the growth of vortex core oscillations toward large amplitude, larger than seen for $\alpha=0.008$ here and that this process begins at 10 G. Thus we infer that, in the present case since no or only small oscillations are seen, Walker breakdown has not been reached for any of the wires (although it may be about to ensue for $\alpha=0.008$). Since 11 G applied at 22.5° to the wire corresponds to a longitudinal component of 10 G and a transverse component of 4 G, and $M_x(t)$ is very similar for the two cases (i) 10 G along the wire and (ii) 11 G applied at 22.5° to the wire direction [see Fig. 8(c)], we conclude that the transverse component of the field has little effect on the motion of the vortex wall. We also conclude that since the vortex core remains closer to the center of the wire as α increases and Walker breakdown requires the sideways movement and oscillation of the vortex core, the Walker breakdown field will increase as the doping increases.

We close this section by offering an empirical explanation for the difference in depinning field between the two VW types and the narrowing of this difference as the Ho content increases [recall Figs. 5(a) and 5(b)]. Both the simulations of DW motion [Fig. 8(b)] and the simulations of DW depinning of both VW types show that for sufficiently small α the vortex core moves toward the leading edge of the DW, requiring the expansion of the rear part of the VW. In the clockwise (counterclockwise) VW, the magnetization in the expanding rear part is aligned with (opposed to) the transverse field component (see Fig. 4 for a depiction), so the depinning of the clockwise (counterclockwise) VW should be easier (more difficult). Meanwhile as the Ho doping increases the vortex core remains closer to the wire center and the expansion of the rear part of the VW becomes less important. Thus for high doping the clockwise and counterclockwise VWs end up with a similar energy barrier for depinning.

V. CONCLUSIONS

In summary, we find that Ho doping of Py wires and the consequent increase in damping α reduces the DW mobility but that $\mu(\alpha)$ only adheres to the prediction of the 1D model for large α. The discrepancy between theory and experiment can be understood using micromagnetic simulations, which show that only for large α can the DW be approximated by a point particle and the 1D model applied. For small α the DW spin structure undergoes periodic distortions that lead to a smaller mobility than predicted. We deduce from the simulations that the onset of Walker breakdown is delayed with increasing doping, due to the increased stability of the DW structure. Finally, the distributions of DW depinning fields, which display distinct channels due to the different meta-

stable states of the DWs, change with the doping due to the changing probability of the initial DW type and the modified α and M_S.

We conclude that doping Py wires with Ho enables control over many aspects of DW propagation, including depinning, mobility and Walker breakdown. This is very important in view of devices that seek to controllably propagate DWs in a viscous regime where their spin structure is preserved. We note that other rare earths such as Gd, Tb, and Dy may have the same or enhanced effects.[24,26,34]

ACKNOWLEDGMENTS

The authors thank U. Rüdiger at Universität Konstanz for his encouragement. This work was supported by the Deutsche Forschungsgemeinschaft (Grants No. SPP 1133, No. SFB 767, and No. KL1811), the EU (Human Resources and Mobility Programme and ERC Starting Grant MASPIC No. ERC-2007-Stg 208162), the Landesstiftung Baden-Württemberg via the Kompetenznetz "Funktionelle Nanostrukturen," Diamond Light Source, Didcot, U.K. [Figs. 1 and 3], Elettra Synchrotron Light Source, Trieste, Italy [Fig. 3], and Swiss Light Source, Paul Scherrer Institut, Villigen, Switzerland [Fig. 3]. P.M. thanks the Stiftung der deutschen Wirtschaft. The research at Elettra has received funding from the European Community's 6th and 7th Framework Programmes (I3:IA-SFS, and ELISA Contract No. 226716).

*Present address: School of Physics and Astronomy, University of Leeds, Leeds LS2 9JT, UK; t.a.moore@leeds.ac.uk

†Also at SwissFEL, Paul Scherrer Institut, 5232 Villigen PSI, Switzerland and Laboratory for Nanomagnetism and Spin Dynamics, Ecole Polytechnique Fédérale de Lausanne, 1015 Lausanne, Switzerland.

‡Also at Fachbereich Physik, Universität Konstanz, Universitätsstrasse 10, 78457 Konstanz, Germany.

§Present address: Departament de Fisica Fonamental i Institut de Nanociència i Nanotecnologia, Universitat de Barcelona, 08027 Barcelona, Spain.

[1] A. Thiaville and Y. Nakatani, *Spin Dynamics in Confined Magnetic Structures III* (Springer, New York, 2006).

[2] L. Thomas and S. S. P. Parkin, *Handbook of Magnetism and Advanced Magnetic Materials* (Wiley, New York, 2007).

[3] D. A. Allwood, G. Xiong, C. C. Faulkner, D. Atkinson, D. Petit, and R. P. Cowburn, Science **309**, 1688 (2005).

[4] S. S. P. Parkin, M. Hayashi, and L. Thomas, Science **320**, 190 (2008).

[5] R. D. McMichael and M. J. Donahue, IEEE Trans. Magn. **33**, 4167 (1997).

[6] M. Kläui, J. Phys.: Condens. Matter **20**, 313001 (2008).

[7] T. Ono, H. Miyajima, K. Shigeto, K. Mibu, N. Hosoito, and T. Shinjo, Science **284**, 468 (1999).

[8] D. Atkinson, D. A. Allwood, G. Xiong, M. D. Cooke, C. C. Faulkner, and R. P. Cowburn, Nature Mater. **2**, 85 (2003).

[9] N. L. Schryer and L. R. Walker, J. Appl. Phys. **45**, 5406 (1974).

[10] A. P. Malozemoff and J. C. Slonczewski, *Magnetic Domain Walls in Bubble Materials* (Academic Press, New York, 1979).

[11] J.-Y. Lee, K.-S. Lee, S. Choi, K. Y. Guslienko, and S.-K. Kim, Phys. Rev. B **76**, 184408 (2007).

[12] G. S. D. Beach, C. Nistor, C. Knutson, M. Tsoi, and J. L. Erskine, Nature Mater. **4**, 741 (2005).

[13] M. Hayashi, L. Thomas, C. Rettner, R. Moriya, and S. S. P. Parkin, Nat. Phys. **3**, 21 (2007).

[14] M. Hayashi, L. Thomas, C. Rettner, R. Moriya, and S. S. P. Parkin, Appl. Phys. Lett. **92**, 112510 (2008).

[15] J. Yang, C. Nistor, G. S. D. Beach, and J. L. Erskine, Phys. Rev. B **77**, 014413 (2008).

[16] S. Glathe, R. Mattheis, and D. V. Berkov, Appl. Phys. Lett. **93**, 072508 (2008).

[17] S.-K. Kim, J.-Y. Lee, Y.-S. Choi, K. Y. Guslienko, and K.-S. Lee, Appl. Phys. Lett. **93**, 052503 (2008).

[18] J.-Y. Lee, K.-S. Lee, and S.-K. Kim, Appl. Phys. Lett. **91**, 122513 (2007).

[19] A. Kunz and S. C. Reiff, Appl. Phys. Lett. **93**, 082503 (2008).

[20] M. T. Bryan, T. Schrefl, D. Atkinson, and D. A. Allwood, J. Appl. Phys. **103**, 073906 (2008).

[21] E. R. Lewis, D. Petit, A.-V. Jausovec, L. O'Brien, D. E. Read, H. T. Zeng, and R. P. Cowburn, Phys. Rev. Lett. **102**, 057209 (2009).

[22] Y. Nakatani, A. Thiaville, and J. Miltat, Nature Mater. **2**, 521 (2003).

[23] M.-Y. Im, L. Bocklage, P. Fischer, and G. Meier, Phys. Rev. Lett. **102**, 147204 (2009).

[24] W. Bailey, P. Kabos, F. Mancoff, and S. Russek, IEEE Trans. Magn. **37**, 1749 (2001).

[25] L. Bocklage, B. Krüger, R. Eiselt, M. Bolte, P. Fischer, and G. Meier, Phys. Rev. B **78**, 180405 (2008).

[26] G. Woltersdorf, M. Kiessling, G. Meyer, J.-U. Thiele, and C. H. Back, Phys. Rev. Lett. **102**, 257602 (2009).

[27] P. Möhrke, T. A. Moore, M. Kläui, J. Boneberg, D. Backes, S. Krzyk, L. J. Heyderman, P. Leiderer, and U. Rüdiger, J. Phys. D **41**, 164009 (2008).

[28] M. Hayashi, L. Thomas, C. Rettner, R. Moriya, X. Jiang, and S. S. P. Parkin, Phys. Rev. Lett. **97**, 207205 (2006).

[29] T. A. Moore *et al.*, J. Magn. Magn. Mater. **322**, 1347 (2010).

[30] http://math.nist.gov/oommf

[31] T. A. Moore *et al.*, Phys. Rev. B **80**, 132403 (2009).

[32] The simulations were carried out using LLG (http://llgmicro.home.mindspring.com).

[33] H. Min, R. D. McMichael, M. J. Donahue, J. Miltat, and M. D. Stiles, Phys. Rev. Lett. **104**, 217201 (2010).

[34] S. Lepadatu, J. Claydon, D. Ciudad, A. Naylor, C. Kinane, S. Langridge, S. Dhesi, and C. Marrows, Appl. Phys. Express **3**, 083002 (2010).